Shell-model study on properties of proton dripline nuclides with $Z, N = 30$–50 including uncertainty analysis*

Bo-Shuai Cai(蔡博帅)[1] Guang-Shang Chen(陈广尚)[1] Cen-Xi Yuan(袁岑溪)[1†] Jian-Jun He(何建军)[2,3‡]

[1]Sino-French Institute of Nuclear Engineering and Technology, Sun Yat-Sen University, Zhuhai 519082, China
[2]Key Laboratory of Beam Technology and Materials Modification of Ministry of Education, College of Nuclear Science and Technology, Beijing Normal University, Beijing 100875, China
[3]Beijing Radiation Center, Beijing 100875, China

Abstract: The binding and proton separation energies of nuclides with $Z, N = 30 - 50$ are investigated based on the shell model, with an uncertainty analysis via statistical methods. Several formulas are used to obtain the binding and proton separation energies according to shell-model calculations. The non-parametric bootstrap method is applied to establish an uncertainty decomposition and recomposition framework. Moreover, this is used to estimate the stability of proton(s) emission for each nuclide. Two formulas for calculating the binding energies with a systematic uncertainty of ~ 0.3 MeV are proposed, and a reliable extrapolation ability is examined. These binding energy formulas deduce similar forms for their respective S_p and S_{2p} energies, which predict the extension of the nuclear boundary of this region. A good description of the binding and proton separation energies is provided. The one- and two-proton separation energies and partial half-lives of proton emission are predicted, thus revealing a new dripline. Furthermore, there are 30 unstable nuclides predicted to be bound against proton(s)-emission. These nuclear properties will be useful in nuclear astrophysics.

Keywords: shell model, proton dripline, uncertainty analysis

DOI: 10.1088/1674-1137/ac6cd7

I. INTRODUCTION

An accurate description of the synthesis of heavy elements in the Universe is a prominent topic open to investigation in the field of nuclear astrophysics, and the type of particles involved in nuclear processes is among the foundations of this investigation [1, 2]. Although the majority of heavy elements are produced via two neutron-induced processes, known as slow (s) and rapid (r) processes [3, 4], there are 35 neutron-deficient stable nuclei (from ^{74}Se to ^{196}Hg), the so-called p nuclei, that cannot be created in these scenarios. These are related to the p-process (or γ-process) with photodisintegration reactions of (γ, n), (γ, p), and (γ, α) [5]. With the exception of nucleosynthesis in nature, there are roughly 7000 possible candidates in the nuclear landscape. However, to date, only roughly 3000 nuclides have been identified, and the vast territory remains to be explored [6−8]. The location of the dripline, defined unambiguously by the nucleon or two-nucleon separation energies [9], depicts the boundary of the nuclear landscape, which is essential for understanding the relationships between the total number of nuclides and the nuclear force [10].

The masses and half-lives of nuclei are important inputs in nuclear astrophysics; therefore, accurate measurements for nuclei are of significant importance. Unfortunately, the measurement of unknown nuclear masses is not always feasible, even with the latest experimental technology. Experimentally, only the neutron dripline of nuclides with $Z \leqslant 10$ have been determined [11]. Thus, theoretical models become crucial for evaluating and predicting unknown masses.

Various mass models have been proposed and corrected in the last several decades. Myers and Swiatecki developed the semi-empirical droplet model of nuclear masses and deformations [12, 13]. The finite-range droplet model, which was developed from a Yukawa-plus-exponential macroscopic model (finite-range liquid-drop model) and a folded-Yukawa single-particle potential for microscopic energy, was proposed by Möller *et al.* in 1981 and corrected in the following years [14−19]. In addition, Hartree-Fock-Bogoliubov theory has been ap-

Received 17 January 2022; Accepted 5 May 2022; Published online 17 June 2022

* Supported by the National Natural Science Foundation of China (11775316, 11825504, 11961141004), the Tip-top Scientific and Technical Innovative Youth Talents of Guangdong special support program (2016TQ03N575), the Guangdong Major Project of Basic and Applied Basic Research (2021B0301030006)

† E-mail: yuancx@mail.sysu.edu.cn
‡ E-mail: hejianjun@bnu.edu.cn

plied to the determination of nuclear masses, and numerous versions have been developed using the Skyrme-type and Gogny-type effective interactions [20–22]. Furthermore, time-dependent Hartree-Fock has been used to describe multinucleon transfer dynamics [23].

In this paper, we conduct a shell-model study on the proton dripline properties of nuclides with $Z,N = 30-50$, which are of importance in astrophysical *v*p-processes. In addition, several nuclei are important in Type I X-ray bursts [24, 25]. A full f_5pg_9 shell model calculation is applied to investigate the binding energies, proton separation energies, and proton dripline properties (including the partial half-lives of proton emission) of these exotic nuclei. The formulas for energy calculation are introduced in Sec. II.A. Furthermore, the confidence of our results is also examined with an uncertainty decomposition framework [28] based on the bootstrap method [29, 30]; this framework is presented in Sec. II.B. Finally, the results are discussed in Sec. III.

II. FORMULAS AND STATISTIC METHOD

A. Calculation of binding and separation energies

In recent years, several properties of light proton-rich nuclei have been studied via experiments, and the shell model has provided reasonable theoretical descriptions of, e.g., isospin asymmetry [31, 32], β-delayed proton(s) emission [33, 34], β-decay spectroscopy [35, 36], the exotic β-γ-α decay mode of ^{20}Na [37], and the four-proton unbound nucleus ^{18}Mg [38]. In neutron-deficient heavy nuclei, the shell model effectively describes the α-decay of the lightest isotope of U [39] and isomeric states of ^{218}Pa [40] and ^{213}Th [41]. For medium mass nuclei, investigations are located mostly in neutron-rich nuclei [42–44] and neutron-deficient nuclei with $Z \leqslant N$ [45–47]; this rarely exceeds $Z = N$.

The shell model provides many descriptions of nuclear spectroscopic properties but rarely investigates the binding energy. A reasonable choice of effective interaction is key to performing shell-model calculations. Through the interaction, shell-model calculations provide the valence part of the binding energy without considering the Coulomb interaction. This is noted as $E_{\rm BE,SM}(Z,N)$, where $Z(N)$ denotes the proton (neutron) number. The effective interaction JUN45, which was proposed by Honma *et al.* via fitting to the experimental data of selected nuclides in the f_5pg_9 shell model space consisting of four single-particle orbits $p_{3/2}$, $f_{5/2}$, $p_{1/2}$, and $g_{9/2}$ [48], is used in the present study to calculate $E_{\rm BE,SM}(Z,N)$. To estimate the binding energy based on the shell model, several corrections should be considered. In 1997, Herndl and Brown [49] used an overall constant (cst) and four terms, linear and quadratic, for the number of valence protons and neutrons:

$$\begin{aligned} E_{\rm BE}(Z,N) =& E_{\rm BE,SM}(Z,N) + cst + a(Z-28) \\ &+ b(Z-28)^2 + c(N-28)^2 + d(N-28), \end{aligned} \quad (1)$$

where a, b, c, and d are fitting parameters. This form is equivalent to the combination of the two body Coulomb interaction and a small variation in the nuclear size and mass [49].

Analogous of Eq. (1), one can construct a quadratic formula for the binding energy of a certain nuclide by fixing the constant term of the original formula with the binding energy of ^{56}Ni:

$$\begin{aligned} E_{\rm BE}(Z,N) =& E_{\rm BE,SM}(Z,N) + E_{\rm BE}(^{56}{\rm Ni}) + a(Z-28) \\ &+ b(Z-28)^2 + c(N-28)^2 + d(N-28). \end{aligned} \quad (2)$$

The correction for the Coulomb energy is included in the a and b terms. In addition, the single-particle energies of the core, which remain unchanged for all nuclides, may actually depend on the number of valence nucleons and should be compensated for by introducing additional terms to Z and N, as suggested in Eq. (2). Through the fitting results, we suggest replacing the last term of Eq. (2) with the difference between valence protons and neutrons:

$$\begin{aligned} E_{\rm BE}(Z,N) =& E_{\rm BE,SM}(Z,N) + E_{\rm BE}(^{56}{\rm Ni}) + a(Z-28) \\ &+ b(Z-28)^2 + c(N-28)^2 + d(Z-N)^2. \end{aligned} \quad (3)$$

Moreover, the sum of the last two terms and the residuals of Eqs. (2) and (3) reveals a hyperboloid-like distribution. Thus, it is approached with the term $(Z-30)(Z-2N+50)$:

$$\begin{aligned} E_{\rm BE}(Z,N) =& E_{\rm BE,SM}(Z,N) + E_{\rm BE}(^{56}{\rm Ni}) + a(Z-28) \\ &+ b(Z-28)^2 + c(Z-30)(Z-2N+50). \end{aligned} \quad (4)$$

Furthermore, Caurier *et al.* [50] proposed a correction including a modified Coulomb energy term and a monopole expression:

$$E_{\rm BE}(Z,N) = E_{\rm BE,SM}(Z,N) + E_{\rm BE}(^{56}{\rm Ni}) + E_{\rm C} + E_{\rm M}, \quad (5)$$

with

$$\begin{aligned} E_{\rm C} =& a(Z-28) + b(Z-28)(Z-29) + c(Z-28)(N-28), \\ E_{\rm M} =& d(A-56) + e(A-56)(A-57) + f\left(T(T+1) - \frac{3}{4}(A-56)\right), \end{aligned}$$

where T is the isospin of the nuclide, and A is the mass number. It is found that Eqs. (3) and (5) are relatively similar. The difference between them is a term involving the gap of the total isospin. When focusing on the ground state property, a general rule is that $T \approx T_3 \propto |N-Z|$. Thus, the term involving the isospin could also be absorbed in the quadratic form of nucleon numbers.

Nucleon separation energies can be easily calculated via the binding energy using the following formulas: $S_p(Z,N) = E_{\rm BE}(Z,N) - E_{\rm BE}(Z-1,N)$ and $S_{2p}(Z,N) = E_{\rm BE}(Z,N) - E_{\rm BE}(Z-2,N)$. From Eqs. (3) and (4), the general forms of S_p and S_{2p} are deduced as

$$S_p(Z,N) = E_{\rm BE,SM}(Z,N) - E_{\rm BE,SM}(Z-1,N) + aZ + bN + d, \tag{6}$$

$$S_{2p}(Z,N) = E_{\rm BE,SM}(Z,N) - E_{\rm BE,SM}(Z-2,N) + aZ + bN + d. \tag{7}$$

Although the quadratic term, $c(Z-N)^2$, disappears by subtracting the two binding energies, it exhibits a correlation with the residuals of Eqs. (6) and (7). After reintroducing this term,

$$S_p(Z,N) = E_{\rm BE,SM}(Z,N) - E_{\rm BE,SM}(Z-1,N) + aZ + bN + c(Z-N)^2 + d, \tag{8}$$

$$S_{2p}(Z,N) = E_{\rm BE,SM}(Z,N) - E_{\rm BE,SM}(Z-2,N) + aZ + bN + c(Z-N)^2 + d, \tag{9}$$

perform well to describe the experimental data with lower uncertainties, as listed in Table 1. Furthermore, the value (uncertainty) of the fitting parameter b significantly decreases (increases) after the reintroduction of $c(Z-N)^2$, which reveals the redundancy and unreliability of b. The term bN is no more robust in Eqs. (8) and (9) and will increase the statistical uncertainty of the formulas. As expected, removing this term makes the following formulas perform better:

$$S_p(Z,N) = E_{\rm BE,SM}(Z,N) - E_{\rm BE,SM}(Z-1,N) + aZ + c(Z-N)^2 + d, \tag{10}$$

$$S_{2p}(Z,N) = E_{\rm BE,SM}(Z,N) - E_{\rm BE,SM}(Z-2,N) + aZ + c(Z-N)^2 + d. \tag{11}$$

The performance of these formulas for the binding and separation energies is investigated via application of the bootstrap method, which is introduced in the subsequent section.

B. Framework of the uncertainty analysis

The total uncertainty of a formula is composed of the experimental, statistical, and systematic uncertainties [26, 27]. Our previous study [28] detailed the practical steps of the bootstrap method [29, 30] for decomposing and recomposing uncertainties. Recently, Jia *et al.* used this to study the correlation between the parameters of the Woods-Saxon potential and evaluate the uncertainty of

Table 1. Fitting parameters, decomposed uncertainties for experimentally determined nuclides, and recomposed uncertainties for the extrapolation of the binding energy, S_p and S_{2p} formulas with standard deviation. The unit is MeV.

	$\sigma_{\rm total}$ *	$\sigma_{\rm stat}$ *	$\sigma_{\rm sys}$ *	$\sigma_{\rm total}$ #	$\sigma_{\rm stat}$ #	a	b	c	d	e	f
$E_{\rm BE}$(Eq.(2))	0.731	0.122	0.721	0.774	0.281	−9.15 (5)	−0.0954 (25)	0.0188 (12)	−0.276 (31)	—	—
$E_{\rm BE}$(Eq.(3))	0.316	0.0482	0.312	0.416	0.275	−9.61 (1)	−0.0944 (8)	0.0245 (5)	−0.0262 (9)	—	—
$E_{\rm BE}$(Eq.(4))	0.317	0.0399	0.315	0.374	0.202	−9.12 (1)	−0.0921 (7)	−0.0309 (5)	—	—	—
$E_{\rm BE}$(Eq.(5))	0.305	0.0563	0.300	0.779	0.719	−9.45 (8)	−0.118 (1)	0.425 (98)	0.0221 (158)	−0.0939 (244)	0.363 (96)
S_p(Eq.(6))	0.286	0.0362	0.284	0.294	0.0781	−0.242 (6)	0.0548 (52)	—	−4.28 (19)	—	—
S_p(Eq.(8))	0.276	0.0404	0.273	0.375	0.257	−0.186 (16)	0.00385 (1541)	0.00335 (88)	−4.36 (19)	—	—
S_p(Eq.(10))	0.275	0.0331	0.273	0.278	0.0519	−0.182 (5)	—	0.00359 (27)	−4.36 (19)	—	—
S_p(Eq.(22))	0.231	0.0328	0.228	0.233	0.0447	−0.183 (4)	—	0.00364 (25)	−4.14 (16)	−0.302 (33)	—
$S_{2p(\rm Eq.(7))}$	0.306	0.0449	0.303	0.320	0.102	−0.478 (8)	0.105 (7)	—	−8.36 (22)	—	—
S_{2p}(Eq.9)	0.265	0.0439	0.261	0.390	0.289	−0.360 (19)	−0.00125 (1794)	0.00736 (111)	−8.55 (21)	—	—
S_{2p}(Eq.(11))	0.264	0.0355	0.261	0.267	0.0527	−0.361 (5)	—	0.00729 (34)	−8.55 (20)	—	—

* Calculated uncertainties for these nuclides with experimentally known data.
# Calculated uncertainties for these nuclides without experimentally known data.

the binary cluster model [51]. The benefit of such a method is that all useful statistics can be obtained simultaneously from the parameter space estimated from the resampling of the dataset. Note that the experimental uncertainties of binding and separation energies are neglected here because they are generally (more than 95%) smaller than 0.1 MeV. The residual between the theoretical and experimental data of a nuclide with Z protons and N neutrons is defined as

$$r(Z,N,S_{\mathrm{BS},i}) = y_{\mathrm{cal}}(Z,N,S_{\mathrm{BS},i}) - y_{\mathrm{exp}}(Z,N), \tag{12}$$

where y denotes the corresponding energy, the subscript cal denotes the calculated value, the subscript exp denotes the experimental value, and $S_{\mathrm{BS},i}$ denotes the ith bootstrap sample among the M bootstrap samples, which are of the same sizes as those in the original dataset. In practice, the number of bootstrap samples is set to be $M = 10^6$, which assures a robust estimation of uncertainties. The ordinary least squares method is used to perform the fitting. Under this definition, a positive value of $r(Z,N,S_{\mathrm{BS},i})$ indicates an overestimation, whereas a negative value indicates an underestimation. The statistical uncertainty of a formula for a nuclide is defined by the unbiased standard deviation

$$\hat{\sigma}^2_{\mathrm{stat}}(Z,N) = \frac{1}{M-1}\sum_{i=1}^{M}\left(y_{\mathrm{cal}}(Z,N,S_{\mathrm{BS},i}) - \bar{y}_{\mathrm{cal}}(Z,N)\right)^2, \tag{13}$$

where $\bar{y}_{\mathrm{cal}}(Z,N)$ is the mean of the calculated values for a given nuclide. The global statistical uncertainty of a formula is the root-mean-square (rms) of $\hat{\sigma}_{\mathrm{stat}}(Z,N)$:

$$\hat{\sigma}^2_{\mathrm{stat}} = \frac{1}{K}\sum_{k=1}^{K}\hat{\sigma}^2_{\mathrm{stat}}(Z,N), \tag{14}$$

where K is the number of combinations of protons and neutrons in the dataset.

By ignoring the experimental uncertainty, the systematic uncertainty, which yields the gaps between the calculated and "true" values, is estimated by

$$\begin{aligned}\hat{\sigma}^2_{\mathrm{sys}}(Z,N) &= \left(\sum_{i=1}^{M}\frac{y_{\mathrm{cal}}(Z,N,S_{\mathrm{BS},i})}{M} - y_{\mathrm{exp}}(Z,N)\right)^2 \\ &= \left(\frac{1}{M}\sum_{i=1}^{M} r(Z,N,S_{\mathrm{BS},i})\right)^2,\end{aligned} \tag{15}$$

and the global systematic uncertainty is derived using

$$\hat{\sigma}^2_{\mathrm{sys}} = \frac{1}{K}\sum_{k=1}^{K}\hat{\sigma}^2_{\mathrm{sys}}(Z,N) = \frac{1}{K}\sum_{k=1}^{K}\bar{r}^2(Z,N). \tag{16}$$

The total uncertainty of a property for a nuclide is defined by the rms of the residuals

$$\begin{aligned}\hat{\sigma}^2_{\mathrm{total}}(Z,N) &= \frac{1}{M}\sum_{i=1}^{M} r^2(Z,N,S_{\mathrm{BS},i}) \\ &= \frac{M-1}{M}\hat{\sigma}^2_{\mathrm{stat}}(Z,N) + \hat{\sigma}^2_{\mathrm{sys}}(Z,N),\end{aligned} \tag{17}$$

and then generalized to the entire dataset as

$$\hat{\sigma}^2_{\mathrm{total}} = \hat{\sigma}^2_{\mathrm{sys}} + \hat{\sigma}^2_{\mathrm{stat}}. \tag{18}$$

In addition, the total uncertainty is recomposed as

$$\hat{\sigma}^2_{\mathrm{pred}}(Z,N) = \hat{\sigma}^2_{\mathrm{stat}}(Z,N) + \hat{\sigma}^2_{\mathrm{sys}}, \tag{19}$$

to verify the extrapolation power.

In effect, each time a bootstrap sample is obtained, the original dataset is divided into two parts: 1) the training group, in which nuclides form the bootstrap sample, and 2) the test group, consisting of nuclides not included in the bootstrap sample. For each bootstrap sample, the uncertainty of the training group is

$$\sigma_{\mathrm{tr}}(S_{\mathrm{BS},i}) = \sqrt{\frac{1}{n_{i,\mathrm{tr}}}\sum_{k=1}^{n_{i,\mathrm{tr}}} r^2(Z_k,N_k,S_{\mathrm{BS},i})}, \tag{20}$$

and that of the test group is

$$\sigma_{\mathrm{ts}}(S_{\mathrm{BS},i}) = \sqrt{\frac{1}{n_{i,\mathrm{ts}}}\sum_{k=1}^{n_{i,\mathrm{ts}}} r^2(Z_k,N_k,S_{\mathrm{BS},i})}, \tag{21}$$

where $n_{i,\mathrm{tr}}$ ($n_{i,\mathrm{ts}}$) is the number of nuclides in the training (test) group. In other words, σ_{tr} and σ_{ts} describe the systematic uncertainties of random interpolation and extrapolation. The distribution of the uncertainties of the training and test groups are illustrated in Fig. 1 for the binding energy formulas in Eqs. (3) and (4) and the separation energy formulas in Eqs. (22) and (11). σ_{tr} is located within the distribution of σ_{ts}. Their difference, $\sigma_{\mathrm{tr}} - \sigma_{\mathrm{ts}}$, is located at approximately 0.01. σ_{ts} distributes slightly wider than σ_{tr}; however, this is not statistically significant. The robustness of the systematic uncertainty estimation can be observed through this check. Note that the statistical uncertainty estimation is restricted to the sub-parameter-space of the correction terms because the uncertainty of the JUN45 interaction is not significant, as

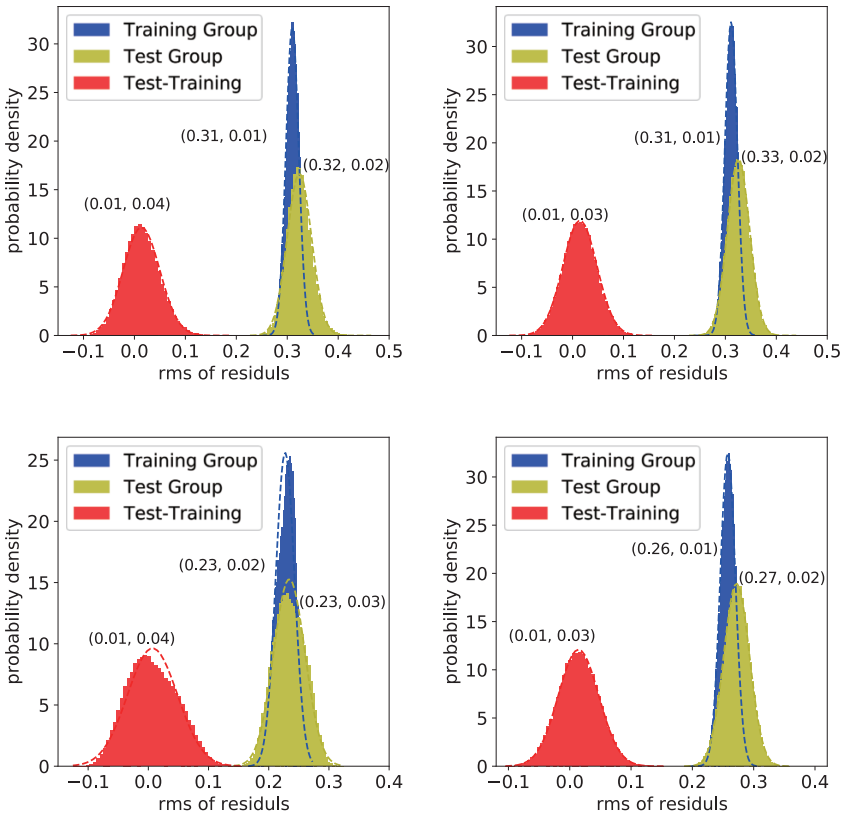

Fig. 1. (color online) Distribution of the uncertainties of the training group, test group, and their difference. The top two are for Eqs. (3) and (4). The bottom two are for Eqs. (22) and (11). The dashed lines are the fitted normal distributions, the parameters of which, i.e., the mean and standard deviation, are listed in the nearby parentheses.

discussed later.

As for the prediction of the stabilities of p-emission and $2p$-emission, i.e., $P(S_p(Z,N)<0)$ and $P(S_{2p}(Z,N)<0)$, one could integrate them directly by assuming normalized distributions for the $S_p(Z,N)$ and $S_{2p}(Z,N)$ energies, which are established from the parameter space of the formula and the corresponding systematic uncertainty.

The results of the application on the binding energy formulas Eqs. (2) –(5) and separation energy formulas Eqs. (6) –(11) are presented and discussed in the subsequent section.

III. RESULTS AND DISCUSSIONS

In this study, experimental data are taken from AME2016 [52] within the nuclear landscape $Z,N\in[30,50]$, corresponding to the f_5pg_9 shell. Two hundred and twenty-one nuclides with experimentally determined (values without #) binding energies are obtained to perform the preliminary computation. For S_p and S_{2p}, the regions are narrowed to $Z,N\in[31,50]$ and $Z,N\in[32,50]$, respectively, including 198 nuclides with experimentally determined S_p and 178 nuclides with experimentally determined S_{2p}. This choice is to avoid uncertainties introduced by the calculation of nuclides with Z,N = 28 and 29. Besides these measurements, there are, in principle, 220 nuclides for $E_{\rm BE}$, 202 nuclides for S_p, and 183 nuclides for S_{2p} to be predicted. In practice, it is not necessary to predict all unknown nuclides in the model space because many of them are far beyond the proton dripline.

A. Binding Energy

The binding energy formulas Eqs. (2)–(5) are applied to the 221 nuclides with measured binding energies via the bootstrap framework. The obtained parameters and uncertainties are summarized in Table 1. As mentioned in Sec. II.A, the effect of the Coulomb interaction is included in the a and b terms. The repulsion between protons will decrease the single particle energy of a proton orbit and the energy released when they form a nucleus, which is consistent with the negative values of a and b. In Eq. (3), the residual is summarized as the competition between the neutron shell effect and isospin effect, which are represented through the square of the valence neutrons and that of the difference between valence protons and neutrons. Because parameters c and d of Eq. (3) are of a similar scale but opposite sign, these two effects compensate for each other when they are far from the proton dripline; this also leads to the equivalence between

Eqs. (3) and (4). The large systematic and statistical uncertainties of Eq. (2), which are approximately twice as large as those of the rest, demonstrate the deficiency of Eq. (2). Eq. (5) achieves the best performance regarding the total and systematic uncertainties, but at the price of six parameters, which results in a significant extrapolation weakness. To control the extrapolating uncertainty in the prediction, the consideration of fewer parameters is recommended.

Figure 2 shows the average of the residuals for each nuclide with experimentally determined binding energies evaluated by AME2016 in the region of $30 \leqslant Z,N \leqslant 50$. The values of the residuals are presented by the gradation of color. Starting from white, the redder the color, the more positive the value, and the bluer the color, the more negative the value. No data have residuals larger than $3\hat{\sigma}_{\rm total}$ or smaller than $-3\hat{\sigma}_{\rm total}$. The extrapolation power is delineated in Fig. 3 by the recomposed uncertainty deduced from Eq. (19). Both formulas exhibit uncertainties that are small near the reached binding energy boundary and increase when moving away. Our predictions for the binding energies are mostly smaller than the extrapolation of AME2016 shown in Table 2. This is consistent with the fact that nuclei near the dripline are less bound than nuclei near the stability line because the extrapolation of AME2016 was obtained under an assumption of a smooth mass surface [53]. Furthermore, more nuclides bound under the energy criterion are predicted in the present study, which awaits experimental examination.

We also attempt another interaction, jj44bpn [54], in the same model space; however, this does not perform well for the description of binding energy. As a quick comparison, $E_{\rm BE,SM}$ of nuclides with $45 \leqslant N \leqslant 50$ or $30 \leqslant Z \leqslant 33$ is calculated through these two interactions. When applied to Eqs. (2)–(5), jj44bpn still has a larger rms of the residuals compared with JUN45, as presented in Table 3. Because jj44bpn does not provide a better description of the binding energy than JUN45, the corresponding results from jj44bpn are not further discussed in the present study.

When constructing the JUN45 interaction, nuclides with $N < 46$ and $Z > 33$ are excluded due to their deformations, the description for which the model space may not be sufficient [48]. To investigate and evaluate the description of nuclides in the middle region, the dataset is

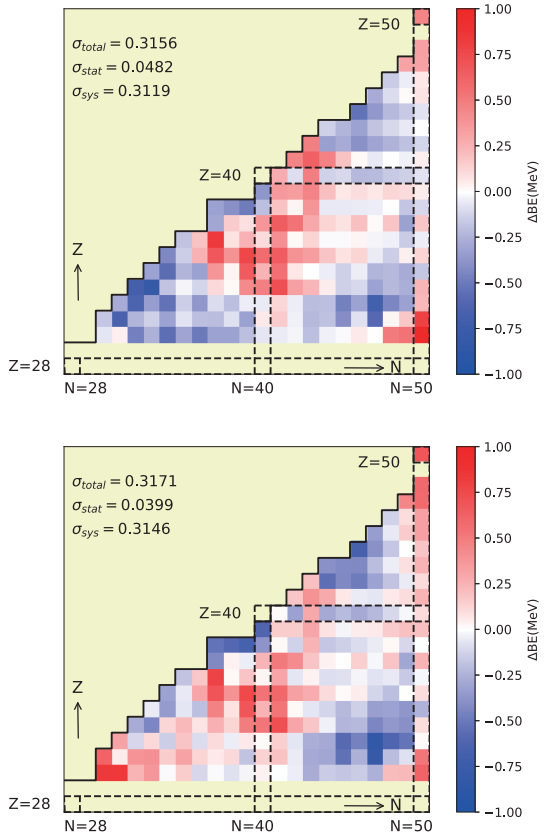

Fig. 2. (color online) Distribution of the mean residual of each nuclide for binding energy formulas Eqs. (3) and (4) in order. The dark solid line shows the measurement boundary of the binding energy in AME2016 [52].

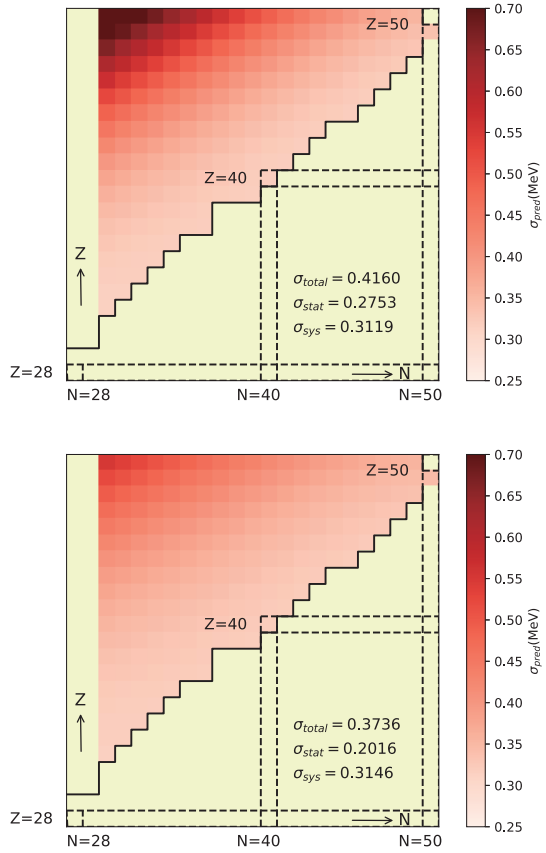

Fig. 3. (color online) Distribution of predictive uncertainty of each nuclide for binding energy formulas Eqs. (3) and (4) in order. The dark solid line shows the measurement boundary of the binding energy in AME2016 [52].

Table 2. Comparison of the predicted ground-state binding energies with those in AME2016 [52] for even-Z nuclides with $N \geqslant Z-6$ and odd-Z nuclides with $N \geqslant Z-5$. The unit of energy is MeV.

Nucl.	Eq. (3)	Eq. (4)	AME2016	Nucl.	Eq. (3)	Eq. (4)	AME2016	Nucl.	Eq. (3)	Eq. (4)	AME2016	Nucl.	Eq. (3)	Eq. (4)	AME2016
^{62}Ge	516.994	517.672	517.142	^{63}As	515.644	516.200	516.159	^{84}Tc	681.878	681.420	682.080	^{85}Tc	698.130	697.735	698.275
^{64}As	529.876	530.363	530.304	^{64}Se	516.288	516.717	516.672	^{86}Tc	712.049	711.722	712.080	^{82}Ru	631.847	631.119	
^{65}Se	530.673	531.043	531.050	^{66}Se	547.138	547.453	547.800	^{83}Ru	647.709	647.043		^{84}Ru	666.221	665.622	
^{65}Br	513.356	513.653		^{66}Br	528.900	529.148		^{85}Ru	681.555	681.025	682.550	^{86}Ru	698.695	698.238	699.438
^{67}Br	545.496	545.698	546.184	^{68}Br	559.822	559.981	560.252	^{87}Ru	712.819	712.439	713.313	^{88}Ru	729.081	728.781	730.224
^{66}Kr	512.830	512.991		^{67}Kr	528.600	528.720		^{89}Ru	741.323	741.106	742.171	^{85}Rh	662.535	661.849	
^{68}Kr	546.273	546.357		^{69}Kr	560.616	560.667	561.177	^{86}Rh	678.669	678.062		^{87}Rh	696.063	695.538	
^{70}Kr	577.440	577.462	577.920	^{69}Rb	543.093	543.054		^{88}Rh	711.244	710.805	711.920	^{89}Rh	727.788	727.438	728.999
^{70}Rb	558.518	558.456		^{71}Rb	575.800	575.718	576.165	^{90}Rh	742.871	742.614	742.950	^{91}Rh	757.236	757.076	757.848
^{72}Rb	590.462	590.363	590.544	^{73}Rb	606.793	606.681	606.338	^{86}Pd	661.508	660.732		^{87}Pd	677.532	676.843	
^{70}Sr	542.659	542.493		^{71}Sr	558.180	558.000		^{88}Pd	696.041	695.444		^{89}Pd	711.176	710.674	
^{72}Sr	576.369	576.178		^{73}Sr	590.968	590.770	591.446	^{90}Pd	729.042	728.639	730.170	^{91}Pd	743.462	743.162	744.471
^{74}Sr	608.019	607.817	608.354	^{73}Y	573.321	573.017		^{92}Pd	760.500	760.305	761.116	^{93}Pd	773.310	773.224	773.667
^{74}Y	588.947	588.644		^{75}Y	606.148	605.851	606.675	^{89}Ag	692.519	691.845		^{90}Ag	708.699	708.130	
^{76}Y	621.059	620.771	621.376	^{77}Y	636.978	636.702	637.406	^{91}Ag	726.633	726.172		^{92}Ag	742.292	741.943	742.900
^{78}Y	650.758	650.498	651.222	^{74}Zr	572.619	572.197		^{93}Ag	759.299	759.064	760.089	^{94}Ag	774.707	774.591	774.372
^{75}Zr	588.291	587.879		^{76}Zr	606.415	606.018		^{95}Ag	789.642	789.648	789.640	^{90}Cd	691.561	690.805	
^{77}Zr	621.419	621.041	622.237	^{78}Zr	638.355	637.998	639.132	^{91}Cd	707.865	707.223		^{92}Cd	726.644	726.120	
^{79}Zr	652.222	651.891	653.093	^{80}Zr	668.167	667.864	668.800	^{93}Cd	742.306	741.903		^{94}Cd	760.402	760.123	761.306
^{77}Nb	603.349	602.848		^{78}Nb	619.281	618.807		^{95}Cd	775.394	775.242	775.865	^{96}Cd	792.748	792.728	792.864
^{79}Nb	636.529	636.086	637.214	^{80}Nb	651.777	651.369	652.080	^{97}Cd	805.940	806.055	805.779	^{93}In	723.213	722.621	
^{81}Nb	667.637	667.267	668.088	^{82}Nb	681.565	681.237	681.830	^{94}In	739.896	739.434		^{95}In	757.960	757.632	
^{78}Mo	602.231	601.620		^{79}Mo	618.297	617.723		^{96}In	774.172	773.981	774.432	^{97}In	791.454	791.403	791.811
^{80}Mo	636.449	635.916		^{81}Mo	651.571	651.082	652.698	^{98}In	806.975	807.069	806.540	^{99}In	822.625	822.866	822.096
^{82}Mo	668.686	668.245	669.366	^{83}Mo	683.032	682.642	683.422	^{94}Sn	722.013	721.348		^{95}Sn	738.737	738.211	
^{84}Mo	698.914	698.578	699.300	^{81}Tc	633.033	632.405		^{96}Sn	757.639	757.257		^{97}Sn	773.837	773.601	
^{82}Tc	649.053	648.478		^{83}Tc	666.556	666.038	667.569	^{98}Sn	792.195	792.109		^{99}Sn	807.901	807.968	807.840

divided into two parts: 1) $N < 45$ & $Z > 33$ and 2) $N \geqslant 45$ or $Z \leqslant 33$. The bootstrap framework is performed separately on these two subsets. The quantification of the deformation effect originates from a cross-extrapolation estimation. As listed in Table 4, compared with the self-estimated result, the systematic uncertainty of the middle region increases significantly when calculated using the parameters estimated with the outer region, and vice versa. This does reveal the difference between nuclides in these two regions. However, the proposed corrections for Eqs. (3) and (4) lead to a trade-off when the full dataset is considered. The uncertainties of the middle region, estimated by parameters fitted to the entire dataset, deviate by less than 0.08 MeV compared with the self-estimated result. Thus, it is reasonable to describe the nuclides in the middle region through the present framework.

Random perturbations in the gaussian form with a σ of 20% ($\mathcal{N}(x,\sigma = 0.2x)$) are applied to the 133 two-body matrix elements (TBMEs). If the uncertainty of the JUN45 interaction remains large, a random perturbation would have a significant probability of obtaining better results for the binding energies. The region is narrowed to the 128 nuclides whose total valence particles and holes are less than 13, corresponding to $A \leqslant 68$ or $A \geqslant 88$ or $N \geqslant Z+10$. Specifically, the application of perturbation to the JUN45 interaction is divided into three groups according to the TBMEs being changed: only the diagonal TBMEs (D), only the non-diagonal TBMEs (ND), and both of these TBMEs (D+ND). Subsequently, the energies relative to the core resulting from the perturbed interactions are inserted into the binding energy formulas to produce a fit, and the rms of the residuals is calculated.

Table 3. Rms of the residuals when JUN45 and jj44bpn are applied to Eqs. (2)–(5) among nuclides with $N \geqslant 45$ or $Z \leqslant 33$.

	Eq. (2)	Eq. (3)	Eq. (4)	Eq. (5)
JUN45	0.586	0.249	0.292	0.249
jj44bpn	0.722	0.873	0.848	0.700

Table 4. Comparison of the decomposed uncertainties estimated by parameters obtained from the middle region ($N < 45$ & $Z > 33$), outer region ($N \geqslant 45$ or $Z \leqslant 33$), and entire region. The parameters of Eq. (3) obtained from the middle region are $a = -9.62(3)$, $b = -0.0858(37)$, $c = 0.0175(18)$, and $d = -0.0108(44)$; those from the outer region are $a = -9.53(2)$, $b = -0.0968(8)$, $c = 0.0229(5)$, and $d = -0.0250(9)$. The parameters of Eq. (4) obtained from the middle region are $a = -9.19(2)$, $b = -0.0873(21)$, and $c = -0.0276(13)$; those from the outer region are $a = -9.10(1)$, $b = -0.0932(7)$, and $c = -0.0305(7)$. The parameters obtained from the entire region are taken from Table 1.

	Objective region	Parameter region	$\sigma_{\rm total}^*$	$\sigma_{\rm stat}^*$	$\sigma_{\rm sys}^*$
Eq. (3)	Middle	Middle	0.317	0.0849	0.305
		Outer	0.557	0.0569	0.554
		Entire	0.379	0.0437	0.377
	Outer	Outer	0.254	0.0473	0.250
		Middle	0.867	0.305	0.812
		Entire	0.286	0.0499	0.281
Eq. (4)	Middle	Middle	0.327	0.0768	0.317
		Outer	0.382	0.0724	0.375
		Entire	0.355	0.0431	0.352
	Outer	Outer	0.295	0.0426	0.292
		Middle	0.461	0.153	0.434
		Entire	0.300	0.0385	0.298

For each group, the perturbation is applied 50 times.

As listed in Table 5 and shown in Fig. 4, the average of the rms of the residuals is larger than that without perturbation for each binding energy formula. However, the influence of the perturbation applied to the non-diagonal TBMEs is weak because the average of the rms of its residuals only exceeds that of the unperturbed one at approximately 0.07 MeV and its distribution is narrow, as illustrated in Fig. 4.

The rms is sensitive to the diagonal TBMEs, as shown through the wide expansion of the distribution in case D and D+ND. Moreover, the rms of the residuals without perturbation drops out of 1.5 (1.75) σ of the distribution when perturbation is applied to the diagonal (all) TBMEs, which implies the significant influence of perturbation and the well fitted diagonal TBMEs of JUN45 interaction. In addition, the number of nuclides, whose spin and parity (J^π) resulting from the perturbed interaction are consistent with those from the observation, is counted. The distribution of the consistency is illustrated in the right panel of Fig. 4. This shows similar results to the perturbation cases for rms. Therefore, the uncertainty of the JUN45 interaction in the energy calculation is shown to be insignificant without perturbation.

Table 5. Comparison of the rms of the residuals when no perturbation is applied to the JUN45 interaction with the average and standard deviation of the rms of the residuals when perturbation is applied to D, ND, and D+ND of the JUN45 interaction among nuclides whose number of valence particles and holes is less than 13.

	Eq. (2)	Eq. (3)	Eq. (4)	Eq. (5)
JUN45	0.651	0.219	0.292	0.216
D	0.778 (201)	0.580 (236)	1.119 (421)	0.464 (159)
ND	0.680 (57)	0.290 (58)	0.359 (62)	0.259 (36)
D+ND	0.787 (181)	0.638 (241)	0.979 (388)	0.505 (148)

The spin and parity of the ground state calculated by the JUN45 interaction ($J^\pi_{\rm JUN45}$) are also compared with those ($J^\pi_{\rm exp}$) from the NNDC. Among the 198 nuclides with determined $J^\pi_{\rm exp}$, there are 137 nuclides whose $J^\pi_{\rm JUN45}$ is consistent with $J^\pi_{\rm exp}$. Moreover, there are 54 nuclides with undetermined $J^\pi_{\rm exp}$. This rarely influences the description of the absolute value of binding energy, which is a bulk property of the nucleus. Generally, nuclear mass models, e.g., the developed semi-empirical droplet model [12, 13], finite-range droplet model [14−19], and application of Hartree-Fock-Bogoliubov theory [20, 21], do not concentrate on the spin and parity.

B. Separation energies, stable possibility, and partial half-lives

Because Eqs. (3) and (4) exhibit good agreement with the experimental binding energies, the deduced formulas are accordingly investigated for the separation energies of the last proton and last two protons, which are expressed by Eqs. (6)−(11). The bootstrap framework is directly applied to the separation energy formulas rather than calculating the separation energies using the binding energy formulas, which can avoid error propagation. Eqs. (6), (8), and (10) and Eqs. (7), (9), and (11) are applied to the 198 S_p and 178 S_{2p} evaluated in AME2016, respectively.

The fitting values of the parameters a, c, and d of the S_{2p} formulas are almost a factor of two larger than those of the corresponding parameters for the S_p formulas. This approximated double relation is mainly caused by the nature of subtracting two protons and one proton in the calculation of S_{2p} and S_p, respectively. Eq. (10) tends to overestimate odd-Z nuclides but underestimate even-Z nuclides, which indicates that the pairing strength may not be well described in shell-model calculations. It is be-

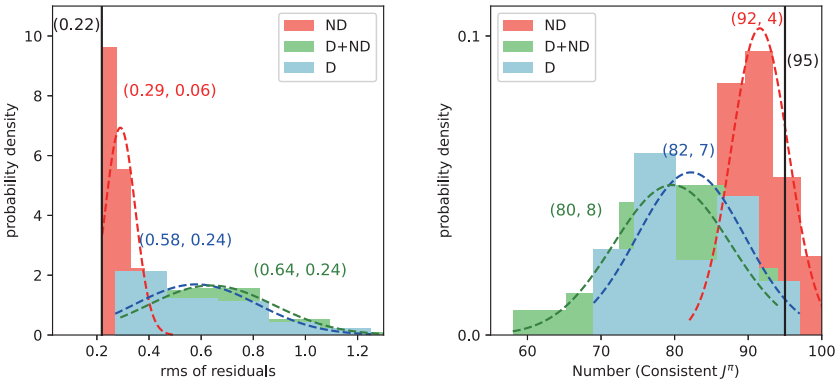

Fig. 4. (color online) Distribution of the rms of the residuals and the number of consistent J^π for perturbations applied to the JUN45 interaction. The dashed lines are the fitted normal distributions, the parameters of which, i.e., the mean and standard deviation, are listed in the nearby parentheses. The vertical black solid line denotes the value when no perturbation is applied, and the black number in parentheses is its corresponding value.

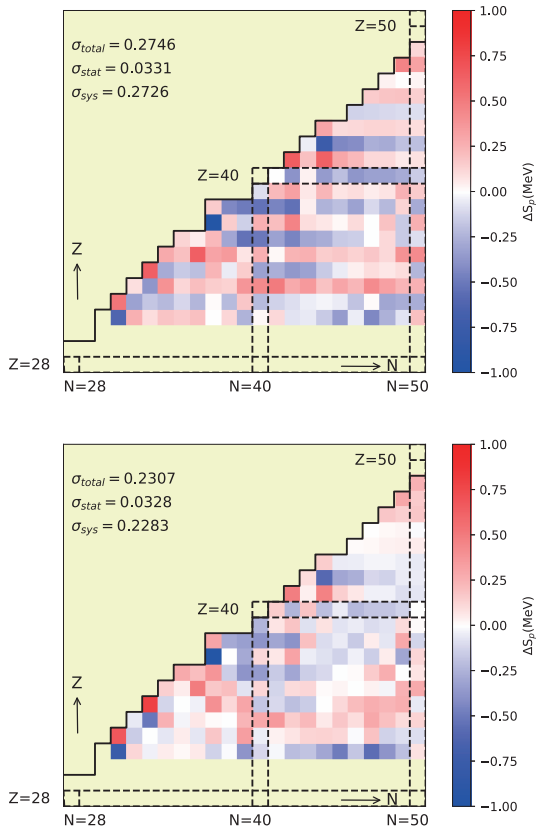

Fig. 5. (color online) Distribution of the mean residual of each nuclide for the S_p formulas Eqs. (10) and (22) in order.

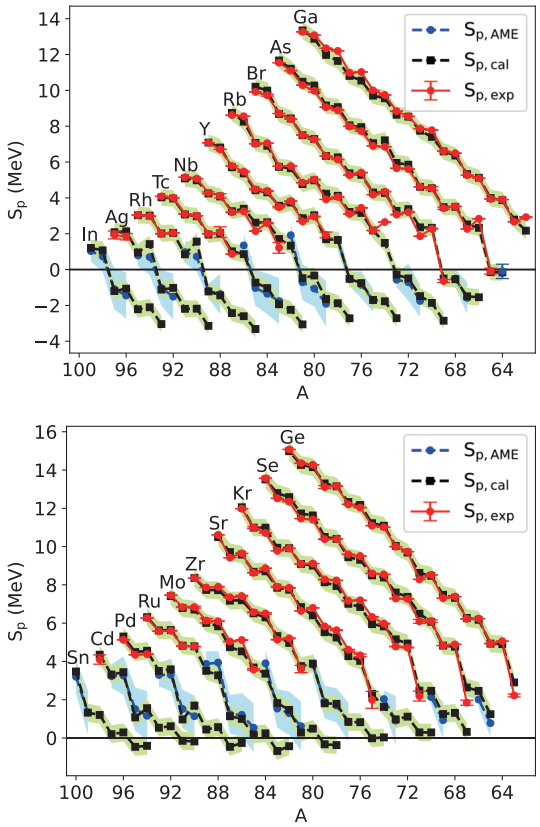

Fig. 6. (color online) S_p calculated in this study and that determined and extrapolated in AME2016. $S_{p,\mathrm{cal}}$ are the values calculated using Eq. (22), $S_{p,\mathrm{exp}}$ are the values determined experimentally in AME2016, and $S_{p,\mathrm{AME}}$ are the extrapolated values in AME2016. The green region, red error bars, and blue region denote the 2σ uncertainties for $S_{p,\mathrm{cal}}$, $S_{p,\mathrm{exp}}$, and $S_{p,\mathrm{AME}}$, respectively.

neficial to introduce an estimation for such extra energy as

$$S_{p(Z,N)} = E_{\mathrm{BE,SM}}(Z,N) - E_{\mathrm{BE,SM}}(Z-1,N) + aZ + c(Z-N)^2 + d + e\delta_Z, \quad (22)$$

where $\delta_Z = 0$ if Z is even and $\delta_Z = 1$ if Z is odd. The correction reduces the uncertainty, as listed in Table 1, and smoothens the residual distribution, as shown in Fig. 5.

Beyond the proton(s) boundary discovered experimentally in AME2016, the separation energies are also calculated theoretically. Figs. 6 and 7 compare the values

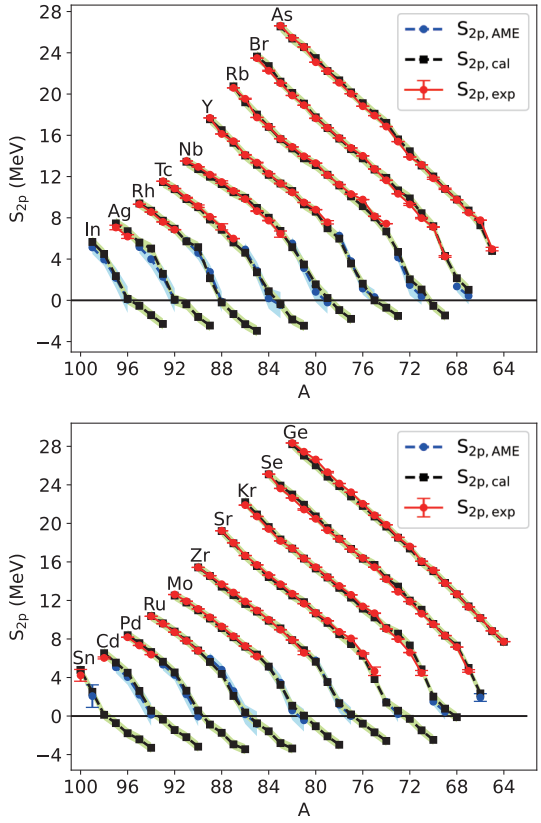

Fig. 7. (color online) S_{2p} calculated in this study and that determined and extrapolated in AME2016. See similar caption of Fig. 6.

of S_p and S_{2p}, respectively, calculated through Eqs. (22) and (11) and those of AME2016. The calculated values agree well with the experimental data, which are mostly located within the 2σ range of the calculations. The present calculations generally agree with the extrapolated values in AME2016, but with smaller uncertainties. This provides important inputs for simulations in nuclear astrophysics and has a significant impact on the understanding of p-process nuclei and their solar abundance. This is because the S_p taken by Pruet *et al.* for the νp-process reaction flow through the Zn-Sn regions for exploring the production of p nuclei in neutrino-driven wind from a young neutron star in Type II supernovae [55] has an extremely large extrapolated uncertainty. They found that the synthesis of p-rich nuclei could be reached up to ^{102}Pd, although their calculations did not reveal efficient production of ^{92}Mo. If the entropy of these ejecta were increased by a factor of 2, the synthesis could extend to ^{120}Te. Further increases in entropy, which might reflect the role of magnetic fields or the vibrational energy input neglected in the hydrodynamical model, resulted in the production of nuclei up to $A \approx 170$.

For the isotope chains of Ge, As, Se, Br, Kr, and Sr, the observed S_p decreases sharply when Z exceeds N. Both the extrapolations in the present study and in AME2016 present such characteristics for other isotopes. For odd-Z nuclides (top of Fig. 6), such a gap leads to the single proton dripline, whereas the pairing of protons makes the single proton dripline of even-Z nuclides farther to reach. This phenomenon also exists for S_{2p}, as shown in Fig. 7. A sharp decrease is shown for As, Se, Br, Kr, and Sr and predicted for other isotopes when Z exceeds N but is smoothed because of the correlation between the two emitted protons. Thus, the proton dripline tends to be extended beyond the $Z = N$ line by the competition between the pairing of protons and Z/N symmetry.

The resampling process in the bootstrap framework estimates the parameter space of Eqs. (22) and (11). Simultaneously, it also estimates the distribution of S_p and S_{2p} for each nuclide. Hence, the possibilities of $S_p < 0$ and $S_{2p} < 0$ for each nuclide are obtained by integrating the estimated normalized distribution. As listed in Table 6, the p- and $2p$- driplines are predicted based on the present calculations.

Thirty candidates that are unstable but bound against both p-emission and $2p$-emission are predicted in Table 6 under the condition of $P(S_p < 0) < 1\% \cap P(S_{2p} < 0) < 1\%$, which are marked in bold in Table 6. Note that $^{100}_{50}$Sn is experimentally S_{2p} known and bound. The present calculation suggests that the drip-lines pass over the $Z = N$ line in this region, which may provide new ideas for waiting points in the path of nucleosynthesis. The separation energies and binding probabilities also provide an opportunity to estimate the pure p-emitters and pure $2p$-emitters in the region $Z, N \in [32, 50]$. Under the conditions $P(S_p < 0) > 99\% \cap P(S_{2p} < 0) < 1\%$ and $P(S_p < 0) < 1\% \cap P(S_{2p} < 0) > 99\%$, nine nuclides (marked with $^{\#}$) and three nuclides (marked with †) are predicted to be pure p-emitters and pure $2p$-emitters, respectively.

With the assumption that the emission is dominated by the channel from ground state to ground state and ignoring the deformation, the corresponding decay half-lives are calculated using a simple law proposed by Qi *et al.* [56]:

$$\log_{10} T_{1/2} = a\chi' + b\rho' + dl(l+1)/\rho' + c, \tag{23}$$

where $\chi' = Z_p Z_d \sqrt{X/Q_p}$, $\rho' = \sqrt{XZ_pZ_d(A_p^{1/3} + A_d^{1/3})}$, and $X = A_pA_d/(A_p + A_d)$. The subscripts p and d denote a proton and daughter nucleus, respectively. The parameters are refit to be $a = 0.4559$, $b = -0.4272$, $d = 2.5706$, $c = -23.08$ based on the data for nuclides with $N < 75$ taken from Ref. [56]. Here, ^{130}Eu and ^{112}Cs are removed because of their large experimental uncertainty and undetermined angular momentum. The uncertainty of separation energy within the 2σ range is accounted for, which denotes a 95% confidence interval. The experimentally determined $J^{\pi}_{g.s.}$ is taken in the partial half-life prediction.

Table 6. Predicted S_p and S_{2p} and the possibility of negative S_p and S_{2p} for experimentally undetermined nuclides, respectively. The partial half-lives, in units of seconds, are calculated for nuclides with $P > 70\%$ using Eq. (23). The half-lives of several ground state nuclides determined experimentally are also listed. Nuclides that are unstable but bound against both p-emission and 2p-emission are marked in bold. Those predicted to be pure p-emitters and pure 2p-emitters are marked with # and †, respectively.

Nucl.	l_p	S_p/MeV	$P(S_p<0)$	$\log_{10}T_{\rm cal}$	$\log_{10}T_{\rm exp}$	l_{2p}	S_{2p}/MeV	$P(S_{2p}<0)$	$\log_{10}T_{\rm cal}$
^{64}As	1	−0.157	75%	$8.6_{-18.2}$					
^{65}Se		1.244	0%						
^{66}Se		2.460	0%				2.352	0%	
^{66}Br	1	−1.545	100%	$-15.8^{+2.4}_{-1.5}$					
^{67}Br#	1	−1.491	100%	$-15.6^{+2.6}_{-1.6}$			1.019	0%	
^{68}Br#	1	−0.540	99%	$-7.3^{+33.9}_{-5.6}$	−7.3 [62]		2.142	0%	
^{67}Kr		0.321	8%						
^{68}Kr		1.312	0%				−0.117	67%	
^{69}Kr		1.252	0%				0.767	0%	
^{70}Kr		2.465	0%				2.016	0%	
^{69}Rb	3	−2.856	100%	$-16.9^{+0.9}_{-0.7}$		2	−1.468	100%	$2.7^{+9.1}_{-5.2}$
^{70}Rb	1	−1.859	100%	$-15.5^{+1.8}_{-1.3}$		2	−0.539	98%	$26.6^{+319.2}_{-17.5}$
^{71}Rb#	3	−1.479	100%	$-13.1^{+2.7}_{-1.7}$			1.047	0%	
^{72}Rb	1	−0.491	98%	$-5.2^{+70.1}_{-6.6}$	$-7.0^{+0.08}_{-0.1}$ [59]		2.038	0%	
^{73}Rb	1	−0.285	89%	$2.1_{-11.7}$	<-7.1 [59]		4.695	0%	
^{70}Sr		0.290	10%			0	−2.477	100%	$-5.7^{+3.7}_{-2.6}$
^{71}Sr		0.294	10%			0	−1.485	100%	$2.8^{+9.1}_{-5.3}$
^{72}Sr		1.115	0%			0	−0.290	87%	$50.2_{-34.3}$
^{73}Sr		0.975	0%				0.550	2%	
^{74}Sr		1.624	0%				1.397	0%	
^{73}Y	4	−2.712	100%	$-14.9^{+1.0}_{-0.8}$		3	−1.511	100%	$4.4^{+9.1}_{-5.3}$
^{74}Y	2	−1.771	100%	$-15.0^{+2.1}_{-1.4}$		1	−0.717	100%	$20.7^{+51.7}_{-13.3}$
^{75}Y	2	−1.698	100%	$-14.7^{+2.3}_{-1.5}$			−0.003	51%	
^{76}Y#	0	−0.752	100%	$-9.2^{+12.0}_{-4.2}$			1.613	0%	
^{77}Y	2	−0.520	99%	$-4.1^{+46.1}_{-6.5}$			3.568	0%	
^{78}Y		1.653	0%				5.980	0%	
^{74}Zr		0.033	44%			0	−2.580	100%	$-5.1^{+3.6}_{-2.6}$
^{75}Zr		−0.014	52%			2	−1.693	100%	$2.5^{+7.6}_{-4.7}$
^{76}Zr		0.825	0%			0	−0.790	100%	$19.2^{+39.6}_{-12.2}$
^{77}Zr		0.840	0%				0.165	26%	
^{78}Zr		1.786	0%				1.335	0%	
^{79}Zr		1.810	0%				3.525	0%	
^{80}Zr		3.887	0%				5.634	0%	
^{77}Nb	2	−2.720	100%	$-17.2^{+1.1}_{-0.8}$		0	−1.798	100%	$1.6^{+7.0}_{-4.4}$
^{78}Nb	1	−1.878	100%	$-15.6^{+2.0}_{-1.4}$		1	−0.948	100%	$15.7^{+25.4}_{-10.0}$
^{79}Nb	1	−1.643	100%	$-14.7^{+2.5}_{-1.6}$			0.225	20%	
^{80}Nb	1	−0.332	93%	$2.5_{-11.1}$			1.553	0%	
^{81}Nb	1	−0.480	98%	$-2.8^{+101.3}_{-7.5}$	<−7.4 [63]		3.475	0%	
^{82}Nb		1.336	0%				5.150	0%	

Continued on next page

Table 6-continued from previous page

Nucl.	l_p	S_p/MeV	$P(S_p<0)$	$\log_{10}T_{\rm cal}$	$\log_{10}T_{\rm exp}$	l_{2p}	S_{2p}/MeV	$P(S_{2p}<0)$	$\log_{10}T_{\rm cal}$
^{78}Mo	2	−0.372	95%	$2.19_{-10.1}$		0	−2.982	100%	$-6.1^{+3.0}_{-2.3}$
^{79}Mo	2	−0.330	92%	$4.1_{-11.4}$		1	−2.105	100%	$-0.3^{+5.4}_{-3.7}$
^{80}Mo		0.489	2%			0	−1.059	100%	$13.9^{+20.2}_{-9.1}$
^{81}Mo		0.284	11%				0.040	44%	
^{82}Mo		1.469	0%				1.069	0%	
^{83}Mo		1.824	0%				3.234	0%	
^{84}Mo		3.360	0%				5.131	0%	
^{81}Tc	1	−3.059	100%	$-18.2^{+0.9}_{-0.7}$		2	−2.462	100%	$-2.0^{+4.2}_{-3.1}$
^{82}Tc	2	−2.246	100%	$-15.7^{+1.5}_{-1.1}$		3	−1.861	100%	$3.5^{+6.9}_{-4.5}$
^{83}Tc	1	−1.936	100%	$-15.4^{+2.0}_{-1.4}$		2	−0.373	92%	$50.1_{-30.4}$
^{84}Tc$^{\#}$	2	−1.031	100%	$-9.7^{+6.5}_{-3.2}$			0.879	0%	
^{85}Tc$^{\#}$	1	−0.724	100%	$-6.7^{+14.7}_{-4.9}$	<−7.4 [63]		2.714	0%	
^{86}Tc		0.863	0%				4.616	0%	
^{82}Ru	1	−0.429	97%	$0.6_{-9.1}$		0	−3.367	100%	$-6.8^{+2.6}_{-2.1}$
^{83}Ru	4	−0.679	100%	$-2.5^{+18.1}_{-5.4}$		2	−2.812	100%	$-3.6^{+3.5}_{-2.6}$
^{84}Ru		0.244	14%			0	−1.586	100%	$6.5^{+9.5}_{-5.7}$
^{85}Ru		0.179	22%			2	−0.754	100%	$26.1^{+51}_{-14.4}$
^{86}Ru		0.996	0%				0.364	8%	
^{87}Ru		1.138	0%				2.085	0%	
^{88}Ru		3.276	0%				4.372	0%	
^{89}Ru		3.509	0%				5.613	0%	
^{85}Rh	4	−3.318	100%	$-15.3^{+0.9}_{-0.7}$		3	−2.955	100%	$-3.3^{+3.3}_{-2.5}$
^{86}Rh	2	−2.603	100%	$-16.3^{+1.3}_{-1.0}$		6	−2.313	100%	$3.3^{+5.0}_{-3.5}$
^{87}Rh	4	−2.427	100%	$-13.5^{+1.4}_{-1.1}$		3	−1.327	100%	$12.3^{+13.8}_{-7.3}$
^{88}Rh	0	−1.441	100%	$-13.0^{+3.5}_{-2.2}$		6	−0.206	78%	$87.9_{-56.7}$
^{89}Rh$^{\#}$	4	−1.223	100%	$-4.6^{+4.8}_{-2.7}$	<−6.9 [58]		2.143	0%	
^{90}Rh		1.563	0%				5.154	0%	
^{91}Rh		0.851	0%				5.716	0%	
^{86}Pd	4	−0.259	87%	$13.7_{-16.1}$		0	−3.445	100%	$-6.2^{+2.7}_{-2.1}$
^{87}Pd	5	−0.462	98%	$5.3_{-8.8}$		5	−2.940	100%	$-1.2^{+3.4}_{-2.6}$
^{88}Pd†		0.568	1%			0	−1.742	100%	$6.1^{+8.4}_{-5.3}$
^{89}Pd		0.444	3%			0	−0.887	100%	$23.1^{+34.4}_{-12.4}$
^{90}Pd		1.696	0%				0.575	1%	
^{91}Pd		0.970	0%				2.628	0%	
^{92}Pd		3.587	0%				4.526	0%	
^{93}Pd		3.507	0%				5.636	0%	
^{89}Ag	4	−3.143	100%	$-14.8^{+1.0}_{-0.8}$		2	−2.445	100%	$0.6^{+4.8}_{-3.5}$
^{90}Ag	4	−2.183	100%	$-12.4^{+1.8}_{-1.3}$		4	−1.616	100%	$10.1^{+10}_{-5.9}$
^{91}Ag	4	−2.192	100%	$-12.5^{+1.8}_{-1.3}$		0	−0.381	92%	$56.3_{-32.9}$
^{92}Ag	2	−1.024	100%	$-8.2^{+7.2}_{-3.5}$			0.053	42%	
^{93}Ag$^{\#}$	4	−1.119	100%	$-6.9^{+6.0}_{-3.1}$	$-6.6^{+0.03}_{-0.03}$ [58]		2.568	0%	

Continued on next page

Table 6-continued from previous page

Nucl.	l_p	S_p/MeV	$P(S_p<0)$	$\log_{10}T_{\rm cal}$	$\log_{10}T_{\rm exp}$	l_{2p}	S_{2p}/MeV	$P(S_{2p}<0)$	$\log_{10}T_{\rm cal}$
^{94}Ag		1.423	0%				5.023	0%	
^{95}Ag		0.958	0%				5.598	0%	
^{90}Cd	4	−0.179	78%	$23.6_{-23.8}$		0	−3.180	100%	$-3.9^{+3.2}_{-2.4}$
^{91}Cd	4	−0.147	74%	$28.8_{-28.3}$		0	−2.195	100%	$2.8^{+5.9}_{-4.1}$
^{92}Cd†		0.612	0%			0	−1.453	100%	$11.9^{+12.5}_{-7.1}$
^{93}Cd		0.537	1%			0	−0.367	92%	$60.1_{-35.1}$
^{94}Cd		1.556	0%				0.550	2%	
^{95}Cd		1.076	0%				2.605	0%	
^{96}Cd		3.439	0%				4.495	0%	
^{97}Cd		3.317	0%				5.545	0%	
^{93}In	4	−3.041	100%	$-14.3^{+1.1}_{-0.9}$		0	−2.288	100%	$2.7^{+5.6}_{-4.0}$
^{94}In	0	−2.105	100%	$-15.0^{+2.0}_{-1.4}$		2	−1.435	100%	$13.5^{+13.2}_{-7.3}$
^{95}In	4	−2.215	100%	$-12.2^{+1.8}_{-1.3}$		0	−0.533	98%	$45.1_{-24.1}$
^{96}In	4	−1.065	100%	$-5.8^{+7.0}_{-3.5}$			0.130	31%	
^{97}In$^{\#}$	4	−1.201	100%	$-7.0^{+5.5}_{-3.0}$			2.349	0%	
^{98}In		1.072	0%				4.494	0%	
^{99}In		1.207	0%				5.657	0%	
^{94}Sn	4	−0.410	96%	7.8_{-11}		0	−3.297	100%	$-3.4^{+3.1}_{-2.5}$
^{95}Sn	0	−0.462	98%	$2.6_{-9.6}$		0	−2.421	100%	$2.2^{+5.3}_{-3.8}$
^{96}Sn		0.291	11%			0	−1.785	100%	$8.7^{+8.9}_{-5.7}$
^{97}Sn		0.199	20%			0	−0.735	100%	$34.2^{+66.4}_{-17.1}$
^{98}Sn		1.205	0%				0.128	32%	
^{99}Sn		1.326	0%				2.515	0%	
^{100}Sn		3.474	0%						

If the experimental data is not available, $J^{\pi}_{g.s.}$ of its mirror partner is used, which is a feasible choice. To the best of our knowledge, there is only one observed mirror-symmetry-violated case for $J^{\pi}_{g.s.}$ [57]. If the $J^{\pi}_{g.s.}$ values of both mirror partners are unknown, the calculated values are used for a referenced estimation.

In recent years, several nuclides in this region have been identified via experiments. Although several nuclides have not been discovered, the limit of their partial half-lives could be estimated. The experimentally estimated ranges of the half-lives of ^{68}Br, ^{72,73}Rb, ^{81}Nb, ^{85}Tc, ^{89}Rh, and ^{93}Ag are summarized in Table 6. These are consistent with the calculated values. $^{93}_{47}$Ag$_{46}$ and $^{89}_{45}$Rh$_{44}$ have been measured to be one-proton emitters but against two proton emission [58], which is qualitatively consistent with the extrapolation results presented in Table 6.

In 2017, the proton emission from the ground-state of ^{72}Rb was measured for the first time [59]. In this study, it is predicted to be proton unbound but two proton bound. Recently, the proton decay of ^{72}Rb was explained by the lower deformation and lower angular momentum barrier [60]. This is consistent with the present calculation under 95% confidence intervals. Its isotope, ^{73}Rb, has not yet been directly measured; however, the upper limit of its half-life was deduced [59]. For ^{73}Rb, the calculated partial half-life has been located beyond the experimental upper limit to date; however, the lower limit estimated theoretically is consistent with this. This is because the calculated S_p value in this study is small with large uncertainties, which induces large uncertainties on the predicted partial half-life.

^{76}Y was identified in Ref. [60]. The β^+ decay with a partial half-life of a few ms was measured as the predominant mode of ^{76}Y, which suggests that this nuclide is possibly proton bound or acquires a sufficiently small proton decay width [60]. In contrast, ^{76}Y is predicted to be proton unbound in the present study, as shown in Table 6. A similar conclusion was drawn in another calculation performed by Kaneko *et al.* [61].

For $^{68}_{35}$Br, its existence was discovered recently, and its half-life was estimated to be 50 ns [62]. This is consistent with the partial half-life estimated in this study.

We suggest further investigations on one proton emitters of ^{68}Br.

IV. CONCLUSION

In summary, based on the nuclear shell model, two formulas with four and three terms, respectively, are recommended to calculate the nuclear binding energies using shell-model binding energies in the $30 \leqslant Z,N \leqslant 50$ region. The contributions of the Coulomb interaction, neutron shell effect, and isospin effect are effectively included. After applying the bootstrap framework, these two formulas have a total uncertainty of approximately 0.3 MeV for nuclides with experimentally known binding energies. The repulsion characteristic of the Coulomb interaction decreases the binding energy as expected. It is found that the neutron shell effect and isospin effect compensate for each other when they are far from the proton dripline. For those without experimental values, the uncertainty of the predicted data is assessed to be approximately 0.4 MeV, which reveals good extrapolation power. In addition, the formulas for S_p and S_{2p} are also recommended with uncertainties less than 0.3 MeV. This shows that the predicted uncertainties of the proton(s) separation energies are mostly smaller than those of the AME2016 extrapolations, and the proton dripline can be extended compared with the boundary reached in experiments. The bootstrap method is developed to estimate the possibilities of the proton(s)-emissions $P(S_p < 0)$ and $P(S_{2p} < 0)$ from the distribution of S_p and S_{2p}. The prediction of the proton(s)-emission property of the nuclides is mostly consistent with the experimental results. Thirty nuclides are suggested to be bound against both p-emission and $2p$-emission. Their spectroscopic properties, such as the β-decay spectrum, must be investigated experimentally and theoretically in future. The energies and partial half-lives predicted in this study can be used as inputs for the simulation of nuclear astrophysics.

ACKNOWLEDGEMENTS

We are grateful for the computational resources from SYSU and the National Supercomputer Center in Guangzhou.

References

[1] C. A. Bertulani, Sci. China-Phys. Mech. Astron. **63**(11), 112063 (2020)
[2] H. L. Liu, D. D. Han, Y. G. Ma *et al.*, Sci. China-Phys. Mech. Astron. **63**(11), 112062 (2020)
[3] F. Käppeler, R. Gallino, S. Bisterzo *et al.*, Rev. Mod. Phys. **83**(1), 157 (2011)
[4] M. Arnould, S. Goriely, and K. Takahashi, Phys. Rep. **450**(4-6), 97 (2007)
[5] M. Arnould and S. Goriely, Phys. Rep. **384**(1-2), 1 (2003)
[6] M. Thoennessen and B. Sherrill, Nature **473**(7345), 25 (2011)
[7] J. Erler, N. Birge, M. Kortelainen *et al.*, Nature **486**(7404), 509 (2012)
[8] W. Nazarewicz, Nat. Phys. **14**(6), 537 (2018)
[9] M. Thoennessen, Rep. Prog. Phys. **67**(7), 1187 (2004)
[10] M. Thoennessen, *The Discovery of Isotopes*, First edition (Switzerland: Springer International Publishing AG Switzerland, 2016)
[11] D. Ahn, N. Fukuda, H. Geissel *et al.*, Phys. Rev. Lett. **123**(21), 212501 (2019)
[12] W. D. Myers and W. J. Swiatecki, Nucl. Phys. **81**(1), 1 (1966)
[13] W. D. Myers, At. Data Nucl. Data Tables **17**(5-6), 411 (1976)
[14] P. Möller and J. R. Nix, At. Data Nucl. Data Tables **26**(2), 165 (1981)
[15] P. Möller and J. R. Nix, Nucl. Phys. A **361**(1), 117 (1981)
[16] P. Möller, W. Myers, W. Swiatecki *et al.*, At. Data Nucl. Data Tables **39**(2), 225 (1988)
[17] P. Möller and J. Nix, At. Data Nucl. Data Tables **39**(2), 213 (1988)
[18] P. Möller, J. Nix, W. Myers *et al.*, arXiv preprint nucl-th/9308022 (1993)
[19] P. Möller, A. J. Sierk, T. Ichikawa *et al.*, At. Data Nucl. Data Tables **109-110**, 1 (2016)
[20] S. Goriely, N. Chamel, and J. Pearson, Phys. Rev. C **88**(6), 061302 (2013)
[21] N. Wang, M. Liu, X. Wu *et al.*, Phys. Lett. B **734**, 215 (2014)
[22] Y. H. Ge, Y. Zhang, and J. N. Hu, Sci. China-Phys. Mech. Astron. **63**(4), 242011 (2020)
[23] Z. J. Wu and L. Guo, Sci. China-Phys. Mech. Astron. **63**(4), 242021 (2020)
[24] H. Schatz and W. J. Ong, Astrophys. J. **844**(2), 139 (2017)
[25] A. Parikh, J. José, C. Iliadis *et al.*, Phys. Rev. C **79**(4), 045802 (2009)
[26] B. S. Cai, G. S. Chen, J. Y. Xu *et al.*, Phys. Rev. C **101**(5), 054304 (2020)
[27] B. Efron, *The jackknife, the bootstrap, and other resampling plans*, First edition (Philadelphia: Society for Industrial and Applied Mathematics, 1982)
[28] B. Efron, Bootstrap Methods: Another Look at the Jackknife. In *Breakthroughs in statistics Vol. II* (New York: Springer-Verlag New York, Inc., 1992), p. 569
[29] J. Lee, X. X. Xu, K. Kaneko *et al.*, Phys. Rev. Lett. **125**(19), 192503 (2020)
[30] H. Jian, Y. F. Gao, F. C. Dai *et al.*, Symmetry **13**(12), 2278 (2021)
[31] X.X. Xu, C. J. Lin, L. J. Sun *et al.*, Phys. Lett. B **766**, 312 (2017)
[32] P. F. Liang, L. J. Sun, J. Lee *et al.*, Phys. Rev. C **101**(2), 024305 (2020)
[33] L. J. Sun, X. X. Xu, C. J. Lin *et al.*, Phys. Rev. C **99**(6), 064312 (2019)
[34] C. G. Wu, H. Y. Wu, J. G. Li *et al.*, Phys. Rev. C **104**(4), 044311 (2021)
[35] Y. B. Wang, J. Su, Z. Y. Han *et al.*, Phys. Rev. C **103**(1), L011301 (2021)

[36] Y. Jin, C. Y. Niu, K. W. Brown *et al*., Phys. Rev. Lett. **127**(26), 262502 (2021)
[37] Z. Y. Zhang, H. B. Yang, M. H. Huang *et al*., Phys. Rev. Lett. **126**(15), 152502 (2021)
[38] M. M. Zhang, H. B. Yang, Z. G. Gan *et al*., Phys. Lett. B **800**, 135102 (2020)
[39] H. B. Zhou, Z. G. Gan, N. Wang *et al*., Phys. Rev. C **103**(4), 044314 (2021)
[40] C. X. Yuan, Z. Liu, F. R. Xu *et al*., Phys. Lett. B **762**, 237 (2016)
[41] Z. Q. Chen, Z. H. Li, H. Hua *et al*., Phys. Rev. Lett. **122**(21), 212502 (2019)
[42] H. Watanabe, C. X. Yuan, G. Lorusso *et al*., Phys. Lett. **823**, 136766 (2021)
[43] X. Y. Yun, D. Y. Pang, Y. P. Xu *et al*., Sci. China-Phys. Mech. Astron. **63**(2), 222011 (2020)
[44] X. Xu, J. H. Liu, C. X. Yuan *et al*., Phys. Rev. C **100**(5), 051303 (2019)
[45] S. Y. Jin, S. T. Wang, J. Lee *et al*., Phys Rev C **104**(2), 024302 (2021)
[46] M. Honma, T. Otsuka, T. Mizusaki *et al*., Phys. Rev. C **80**(6), 064323 (2009)
[47] H. Herndl and B. Brown, Nucl. Phys. A **627**(1), 35 (1997)
[48] E. Caurier, G. Martinez-Pinedo, F. Nowacki *et al*., Phys. Rev. C **59**(4), 2033 (1999)
[49] J. Dobaczewski, W. Nazarewicz, and P. G. Reinhard, J. Phys. G: Nucl. Part. Phys. **41**(7), 074001 (2014)
[50] C. X. Yuan, Phys. Rev. C **93**(3), 034310 (2016)
[51] J. Jia, Y. Qian, and Z. Ren, Phys. Rev. C **104**(3), L031301 (2021)
[52] M. Wang, G. Audi, F. Kondev *et al*., Chin. Phys. C **41**(3), 030003 (2017)
[53] W. J. Huang, G. Audi, M. Wang, *et al*., Chin. Phys. C **41**(3), 030002 (2017)
[54] B. Brown and W. Rae, Nucl. Data Sheets **120**, 115 (2014)
[55] J. Pruet, R. D. Hoffman, S. E. Woosley *et al*., Astrophys. J. **644**(2), 1028 (2006)
[56] C. Qi, D. S. Delion, R. J. Liotta *et al*., Phys. Rev. C **85**(1), 011303 (2012)
[57] D. E. M. Hoff, A. M. Rogers, S. M. Wang *et al*., Nature **580**(7801), 52 (2020)
[58] I. Ćeliković, M. Lewitowicz, R. Gernhäuser *et al*., Phys. Rev. Lett. **116**(16), 162501 (2016)
[59] H. Suzuki, L. Sinclair, P.-A. Söderström *et al*., Phys. Rev. Lett. **119**(19), 192503 (2017)
[60] L. Sinclair, R. Wadsworth, J. Dobaczewski *et al*., Phys. Rev. C **100**(4), 044311 (2019)
[61] K. Kaneko, Y. Sun, T. Mizusaki *et al*., Phys. Rev. Lett. **110**(17), 172505 (2013)
[62] K. Wimmer, P. Doornenbal, W. Korten *et al*., Phys. Lett. B **795**, 266 (2019)
[63] H. Suzuki, T. Kubo, N. Fukuda *et al*., Phys. Rev. C **96**(3), 034604 (2017)